UDK 621.791.725:669.14.018.62
Original scientific article/Izvirni znanstveni članek

ISSN 1580-2949
MTAEC9, 58(1)25(2024)

NUMERICAL MODEL FOR OPTIMIZING THE PARAMETERS FOR LASER-BEAM WELDING OF A HIGH-TEMPERATURE MATERIAL

NUMERIČNI MODEL ZA OPTIMIZACIJO PARAMETROV LASERSKEGA VARJENJA VISOKOTEMPERATURNIH MATERIALOV

Ramaswamy Palanivel[1*], Thiyagarajan Muthu Krishnan[2], Yousef Alqurashi[1,3], Mohammad Abdur Rasheed[4]

[1]Department of Mechanical Engineering, College of Engineering, Shaqra University, Dawadmi, Riyadh 11911, Saudi Arabia
[2]Department of Mechanical Engineering, SRM Valliammai Engineering College, Kattankulathur 603203, Tamil Nadu, India
[3]Saudi Railway Research Group, Department of Mechanical Engineering, College of Engineering, Shaqra University, Dawadmi, Riyadh 11911, Saudi Arabia
[4]Department of Civil Engineering, College of Engineering, Shaqra University, Dawadmi, Riyadh 11911, Saudi Arabia

Prejem rokopisa – received: 2023-09-06; sprejem za objavo – accepted for publication: 2023-12-04

doi:10.17222/mit.2023.990

Ferritic stainless steel (FSS) is one of the high-temperature materials, used in many industries for sustainable applications such as power plants, automotive, offshore and chemical industries. Joining these materials is challenging due to the formation of an intermetallic and the grain growth with high-heat-input welding methods. Laser beam welding (LBW) that uses a low heat input was used successfully to join AISI 409 FSS tubes. In this work the welding speed and focal distance were varied as per a two-factor, three-level face-centred central composite design (FCCCD) to join AISI 409 FSS. A numerical model was developed to correlate the relationship between the ultimate tensile strength (UTS) and LBW process parameters. The validation of the developed model was carried out using the analysis of variance. Both welding speed and focal distance have a significant effect on determining the UTS. The optimised process parameters provided for a better UTS as reported in this paper.

Keywords: laser beam welding, high-temperature materials, ferritic stainless steel, sustainable manufacturing

Feritna nerjavna jekla (FSS, angl.: Ferritic Stainless Steels) so ena izmed mnogih vrst materialov oziroma kovinskih zlitin, ki se uporabljajo pri visokih in povišanih temperaturah v mnogih industrijah kot so naprimer ladjedelništvo, termo- in nuklearne elektrarne ter kemijska industrija za trajnostne aplikacije. Spajanje teh materialov je zahtevno zaradi tvorbe trdih in krhkih intermetalnih spojin ter pretirane rasti kristalnih zrn zaradi velikega vnosa toplote med varjenjem. Varjenje z laserskim snopom (LBW, angl.: laser beam welding) je tehnika pri kateri se uporablja manjši vnos toplote za spajanje cevi iz nerjavnega jekla vrste AISI 409. V tem članku avtorji opisujejo vpliv spreminjanja hitrosti laserskega varjenja in žariščne razdalje na spajanje tri nivojskega dizajna centralno ploskovno centriranega kompozita (CCFC, angl.: three-level central composite face-centred design) iz nerjavnega jekla vrste AISI 409. Avtorji so razvili numerični model za napoved korelacije med končno natezno trdnostjo (UTS, angl.: ultimate tensile strength)in parametri laserskega varjenja. Razviti model so ovrednotili z uporabo tehnike analize variance. Oba izbrana parametra, to je hitrost varjenja in žariščna razdalja imata pomemben vpliv na končno natezno trdnost spoja. V članku avtorji opisujejo postopek optimizacije procesnih parametrov za izboljšanje končne natezne trdnosti spojev izbrane konstrukcije oziroma dizajna.

Ključne besede: lasersko varjenje, visoko temperaturni materiali, feritna nerjavna jekla, trajnostna proizvodnja

1 INTRODUCTION

Ferritic stainless steel (FSS) has a body-centred cubic structure (BCC) at a normal temperature and good corrosion resistance due to 12–25 *w*/% of chromium (Cr), which acts as a protective layer against the atmosphere. Joining FSS tubes is essential for meeting the demand of power plants and petrochemical industries to transfer fluids from one end to another.[1] The weldability of FSS is good with the fusion welding method.[2] Inappropriate fusion welding techniques produce incomplete joints, less penetration and defects that can weaken the joints. A higher amount of heat input restricts the expected joint properties. The growth of grains in the heat-affected zone (HAZ) is higher because of a slower cooling rate.[3] Most of the defects take place due to an insufficient or excess heat input. Also, the joints become weaker due to the formation of intermetallic phases sigma (σ) and chi (χ) with the fusion welding method.[4,5] So, the selection of the joining technique and process parameters is necessary for producing defect-free joints. LBW is an appropriate method for joining FSS because of its merits such as a lower heat input, smaller HAZ, higher production rate and higher level of automation. The joint properties obtained with LBW are determined by the process parameters such as laser power, welding speed, focal distance, pulse width, pulse frequency, etc.[6–8]

RSM is one of the methods based on statistical techniques of DOE, which uses input parameters to investigate the output parameters and optimise the inputs for better outputs or responses. There are different techniques of RSM, of which the central composite face-cen-

*Corresponding author's e-mail:
rpalanivelme@gmail.com (Ramaswamy Palanivel)

tred (CCFC) factorial design technique has more validation with minimum logical experiments.[9] Cao et al.[10] studied the LBW process parameters of 3 mm thick AISI 316L using GA and RBFNN. They found that the laser power and welding speed are the deciding factors for good joint properties. Optimization of process parameters for hybrid laser–TIG welding of 5.6 mm thick AISI316L steel was carried out by Ragavendran et al.[11] They concluded that the pulse frequency, laser power and pulse duration are the significant input parameters for the bead width and depth of penetration. Jiang et al.[12] developed a finite element model to optimise the LBW parameters for 3 mm thick 316L stainless steel. The welding speed, laser power and focal distance were the input parameters, whereas the depth of penetration and bead width were the output parameters for their study. Torabi et al.[13] used the response surface method (RSM) and a simulated annealing algorithm to develop a mathematical model for predicting the UTS of a thin AISI316L sheet after LBW. They concluded that the RSM is one of the best techniques for analysing the interaction between input parameters and responses. The effects of the welding speed, focal distance and laser power of CO_2 laser welding on medium-carbon steel was investigated by Benyounis et al.[14] using the RSM technique. Chatterjee et al.[9] used the DOE technique with an RSM-based face-centred central composite design (FCCCD) matrix to conduct the LBW of 0.45 mm thin sheets of AISI 316. Vahiddastjerdi et al.[15] used the RSM technique for the LBW of high-Mn TWIP steel. They used the laser power, welding speed and spot size as the input parameters and concluded that the laser power had the major influence on defining the UTS responses. Olabi et al.[16] optimised LBW process parameters using the RSM for dissimilar joints between low-carbon steel and austenitic steel AISI316. They reported that the welding speed was the most effective parameter, compared to the laser power and focal position, for defining the weld-bead dimensions and UTS of the joints. Kumar et al.[17] used the RSM to compare the joint properties of AISI304 and AISI 316 stainless steel joined with LBW. They reported that the most significant factor for defining the UTS was the pulse width compared to the welding speed and laser power. Pakmanesh[18] et al. optimized the process parameters to minimise the LBW underfill and undercut defects of 316L stainless steel using RSM. They reported that the laser power had the greatest impact on the defects. Undercut and underfill defects increased with increased pulse duration, frequency and laser power. According to a literature analysis, very limited studies on the LBW of FSS are available. The existing studies only focus on plates. So, in this work the joining of AISI 409 FSS tubes was investigated successfully and the process parameters were optimised using the RSM technique with a FCCCD matrix.

2 EXPERIMENTAL WORK

AISI 409 FSS tubes were 4 mm thick, their outer diameter was 44 mm and the length was 150 mm; a chemical composition (in *w*/%) of 86.39 % Fe, 12.65 % Cr, 0.74 % Mn, 0.46 % Si, 0.11 % Ni, with few traces of Al, Cu, Co, C, P and S was selected for this investigation. The tube edges were cleaned using solvents and clamped firmly to the rotating chuck. The process parameters and their levels were selected based on trial experiments. Based on the process parameters, the FCCCD matrix was selected as presented in **Table 1**. Helium was used as the shielding gas with a gas flow rate of 15 lpm. The angle

Table 1: Laser-welding process-parameter levels along with the FCCCD matrix and response

LBW welding parameter	Levels			
	–1	0	1	
Welding speed, m/min	1.3	2.3	3.3	
Focal distance, mm	13	18	23	
Face-centered central composite design matrix (two parameters, three levels)		Response (ultimate tensile strength, MPa)		Percentage of error (E–P/P) x100
Welding speed (S)	Focal distance (D)	Experimental value (E), MPa	Predicted value (P), MPa	
–1	–1	490	482.77	1.50
1	–1	467	477.05	–2.11
–1	1	484	484.51	–0.11
1	1	460	469.31	–1.98
–1	0	496	490.39	1.14
1	0	470	479.93	–2.07
0	–1	494	501.54	–1.50
0	1	492	498.54	–1.31
0	0	501	506.79	–0.55
0	0	504	506.79	–0.55
0	0	502	506.79	0.24
0	0	504	506.79	–0.55
0	0	504	506.79	–0.55

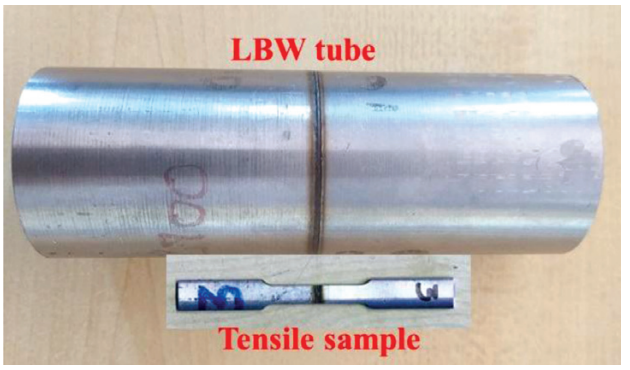

Figure 1: LBW tube with a tensile sample

of incident was normal to the welding. LBW was carried out using a developed design matrix and experimental set-up. A sample of welded tubes is shown in **Figure 1**. Three tensile specimens were extracted from the welded tube as per the ASTM E8M-04 standard and the samples are shown in **Figure 1**. After each tensile test, the UTS average value was recorded as the ultimate tensile strength or response in **Table 1**. Specimens for microstructural studies were prepared as per the standard metallurgical technique. Etching of a prepared specimen was done for 2 min with a mixture of 10 mL glycerol, 5 mL HNO_3 and 15 mL HCl to reveal the microstructures of LBW joints. A field emission scanning electron microscope (FESEM) and electron backscatter diffraction (EBSD) were used to observe the microstructures of the LBW samples. Tensile fracture samples were observed using the FESEM to analyse the mode of fracture.

3 RESULTS

3.1 Development of an RSM-based numerical model

The relationship between the two input parameters (welding speed and focal distance) and the output (the UTS of the LBW joints) were derived from the 13 sets of experimental data using the RSM RSM-based FCCCD matrix. Mathematically, the relationship between the welding speed and focal distance to the response UTS of LBW joints is expressed with Equation (1).

$$\text{UTS} = F\,(S, D) \tag{1}$$

Here, S – welding speed, D – focal distance

The second-order polynomial equation of the UTS of LBW joints with two parameters is Equation (2) below:

$$\text{UTS} = b_0 + b_1 S + b_2 D + b_{11} S^2 + b_{22}\, D^2 + b_{12} SD \tag{2}$$

where b_0 is the constant value; b_1 and b_2 are the first-order terms related to the welding speed and focal distance, respectively; b_{11} and b_{22} are the second-order terms related to the welding speed and focal distance, respectively; b_{12} is the interaction term between the welding speed and focal distance. The above-mentioned coefficients are calculated using Design Expert 13 software and the developed equation in coded form is included in Equation (3).

$$\text{UTS} = 506.79 - 5.23S - 1.5D - 21.63S^2 - 6.75D^2 - \\ - 2.37SD \tag{3}$$

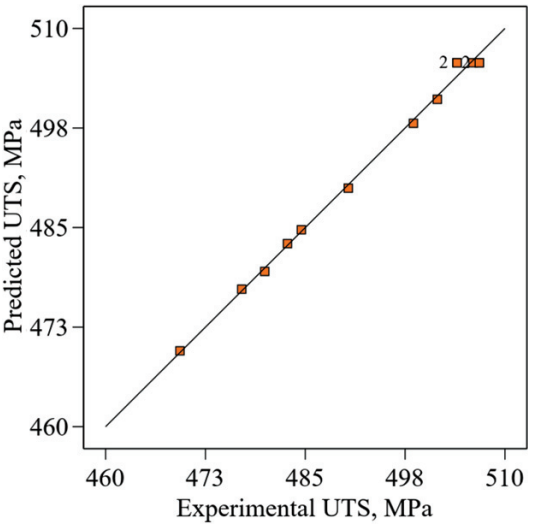

Figure 2: Scatter plot for LBW of the AISI 409 tube

Table 2: ANOVA for second-order quadradic models

Source	Sum of squares	Degrees of freedom	Mean square	F-value	p-value	
Model	2055.22	5	411.04	312.88	< 0.0001	
S	164.12	1	164.12	124.92	< 0.0001	
D	13.50	1	13.50	10.28	0.0149	
SD	22.47	1	22.47	17.10	0.0044	Significant
S^2	1214.64	1	1214.64	924.56	< 0.0001	
D^2	102.47	1	102.47	78.00	< 0.0001	
Residual	9.20	7	1.31			
Lack of fit	1.12	3	0.3731	0.1848	0.9016	
Pure error	8.08	4	2.02			Not significant
Cor. total	2064.41	12				
R^2	Adjusted R^2	Predicted R^2	Adequate precision			
0.9955	0.9924	0.9906	46.44			

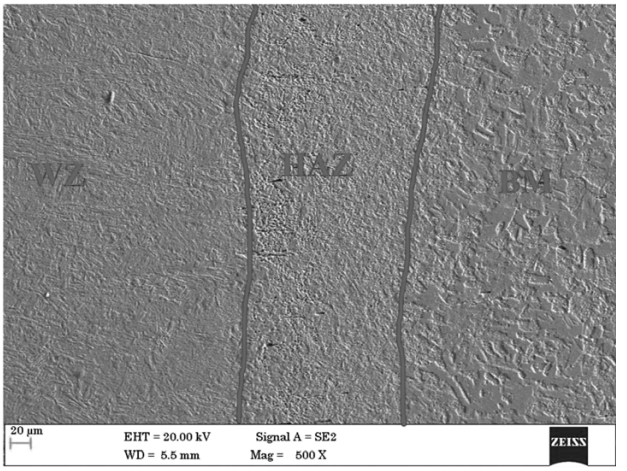

Figure 3: FESEM micrograph of the AISI 409 tube after LBW

3.2 Validation of the developed model using ANOVA

ANOVA was done to validate the developed model and its results are presented in **Table 2**. The developed numerical model F-value of 312.88 infers the model is significant. An F-value this large might arise owing to noise only 0.01 % of the time. In this model, S, D, SD, S^2 and D^2 are considered as the significant terms as their p values are less than 0.05. An insignificant lack of fit is good for any developed numerical model for validation. The R^2 and adjusted R^2 values for the predicted model are in good agreement with each other.

In general, the R^2 and adjusted R^2 values should be 0.6–1; in this case, they are close to 1. The signal-to-noise ratio for the developed numerical model is 46.44, which indicates that the model has an adequate signal. A scatter plot was drawn for the predicted and experimental values and all the values are very close to the 45° line as shown in **Figure 2**. In the light of the above, the developed model is adequate to use.[9,19]

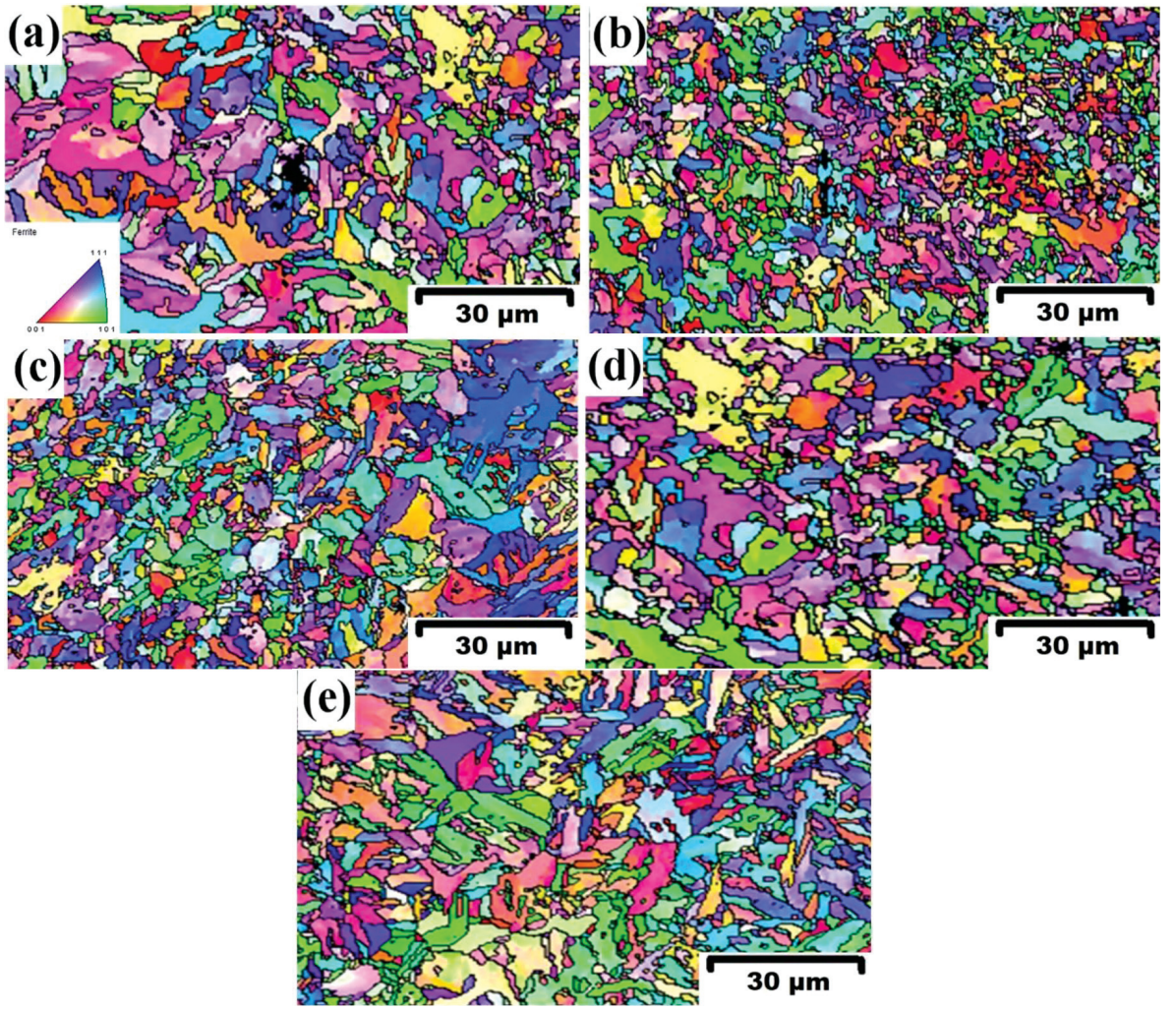

Figure 4: EBSD images of the WZ of the AISI 409 FSS tube: a) welding speed of 1.3 m/min, b) welding speed of 3.3 m/min, c) focal distance of 13 mm, d) focal distance of 23 mm, e) welding speed of 2.3 m/min and focal distance of 18 mm

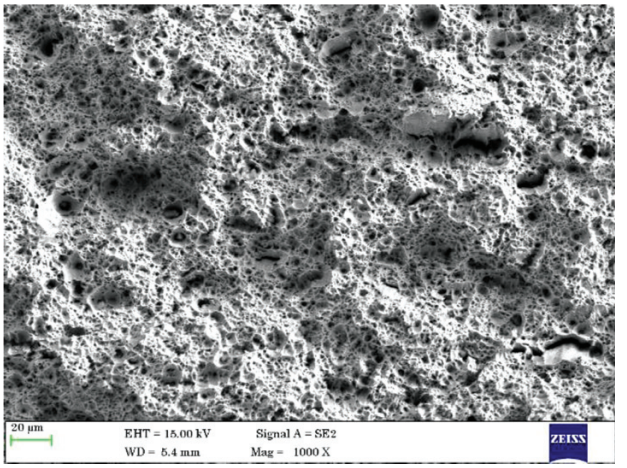

Figure 5: Fracture surface of the AISI 409 FSS tube after LBW with a welding speed of 2.3 m/min and focal distance of 18 mm

3.3 Microstructure

A FESEM micrograph of AISI 409 after LBW is shown in **Figure 3**. Three different zones are observed: the base metal, HAZ and weld zone or fusion zone.

The fusion zone was analysed with EBSD to observe the grain structure and the results are presented in **Figure 4**. The tensile fracture morphology of tensile specimens was also analysed as shown in **Figure 5**.

4 DISCUSSION

4.1 Effect of the welding speed and focal distance

The LBW process parameters including the welding speed and focal distance have an impact on the UTS of the joints as presented in the response and contour graphs in **Figure 6**, depicting the overall relationship between the causes and effects.

The laser welding speed increasing from 1.3 m/min to 2.3 m/min increased the UTS of the LBW joints; later a decrement in the UTS was observed with a further increment in the welding speed from 2.3 m/min to 3.3 m/min. Microstructural variation is seen due to the heat energy variation during the welding (**Figure 3**). The highest heat and related rate of cooling drop as one moves far from the laser beam. The effect of heat energy fades away at a certain distance when the basic-metal grains remain unchanged. It is worth noting that a very small region of the heat-affected zone is observed. In the FZ, a dendric structure is observed. Further, the observed EBSD microstructure of the FZ for different process parameters is shown in **Figure 4**. It is obvious that there is a dendritic microstructure throughout the image. The uneven features within the dendritic structure, in contrast to a well-defined grainy structure, prevented an estimation of the grain size. However, it is noted that as the welding speed increases, the dendritic structure's size becomes more precise. The decrease in the heat input and greater cooling rate may be attributed to this change. The rate at which solidifying steel cools from its molten state to room temperature controls the changes to the dendritic structure.[20] According to **Figure 4**, there is a longer time available for the formation of the dendritic microstructure at 1.3 m/min than at 3.3 m/min. A shorter time is available at higher welding speeds, consuming a larger amount of heat. As a result, the dendritic structure gradually shrinks. The welding speed of 3.3 m/min allows less tensile strength due to an undercut defect formed at the bottom of the weld zone. Lakshminarayanan et al.[21] observed incomplete penetration at higher welding speeds. The lowest welding speed produces a high amount of heat in the weld area, which can create pores. So, high and low welding speeds produce less tensile strength.

An increase in the focal distance from 13 mm to 18 mm leads to an increasing trend of the UTS of the LBW joints, which starts to decrease with an increase from 18 mm to 23 mm. The power density can be changed by the focal distance, also affecting the mode of weld, width

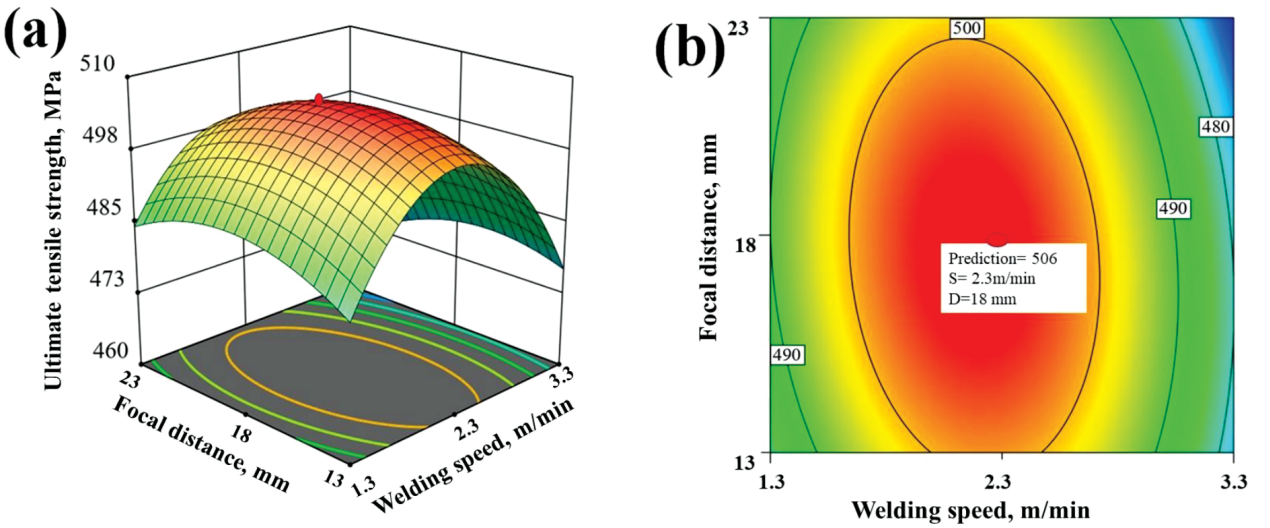

Figure 6: a) Response plot between the welding speed and focal distance, b) contour plot with predicted values for better process parameters

of weld and depth of penetration.[8] Insufficient and excessive penetrations occur at the lowest and highest focal distances, respectively, which may affect the strength of the joints. A fine dendritic structure is observed with the EBSD analysis at a high focal distance due to a low power density, which causes the heat input to decrease and the cooling rate to increase. **Figure 5** shows heavily packed fine voids on the fracture surface. The failure originates from well-developed and interrelated voids. The ductile mode of failure occurs. These striations propagate the fracture further. The collapse, meanwhile, does not occur suddenly, exhibiting the traits of a normal ductile failure.

4.2 Optimisation of LBW process parameters

In order to obtain an optimised process parameter combination for a better UTS of LBW AISI 409, we can use the response and contour graphs developed by the numerical model and presented in **Figure 6**. These response contours can be used for any section of the experimental region to help predict the outcome (UTS).[9] The vertex of the response graph is used for determining the highest attainable UTS. The optimised process parameters are identified visually with the help of the contour graph. It is difficult to develop a contour graph for a second-order model compared to a first-order numerical model. Characterizing a response surface close to a motionless spot may be necessary once it has been located. Characterization entails determining if the motionless spot is a saddle point, maximum or minimum response. Examining it through a contour graph makes categorization easy. The process parameters can be ranked based on the F-ratio calculated using ANOVA. As per the F-ratio, the welding speed has a more significant effect than the focal distance in determining the UTS. The obtained maximum UTS is found to be 506 MPa, corresponding to a welding speed of 2.3 m/min and focal distance of 18 mm.

5 CONCLUSIONS

The conclusions of this research work are as follows:

- Tubes of AISI 409 FSS were joined successfully using LBW.
- The RSM with a face-centered central composite factorial design was suitable for developing a numerical model with minimum logical experiments.
- The welding speed and focal distance have significant effects on the UTS of the AISI 409 FSS tubes.
- EBSD micrographs of the WZ show significant effects of different welding speeds and focal distances.
- The welding speed of 2.3 m/min and focal distance of 18 mm were identified as the best process parameter combination for achieving the maximum UTS of 506 MPa.

Acknowledgment

The authors extend their appreciation to the Deanship of Scientific Research at the Shaqra University, Saudi Arabia, for funding this research work through project number SU-ANN-2023031.

6 REFERENCES

[1] M. A. Khattak, S. Zaman, S. Kazi, H. Ahmed, H. M. Habib, H. M. Alie, M. N. Tamin, Failure investigation of welded 430 stainless steel plates for conveyor belts, Engineering Failure Analysis, 116 (**2020**) 104754, doi:10.1016/j.engfailanal.2020.104754

[2] Z. Dong, Y. Li, B. Lee, A. Babkin, Y. Chang, Research status of welding technology of ferritic stainless steel, The International Journal of Advanced Manufacturing Technology, 118 (**2022**), 2805–2831, doi:10.1007/s00170-021-08128-6

[3] M. Alizadeh-Sh, S. P. H. Marashi, M. Pouranvari, Resistance spot welding of AISI 430 ferritic stainless steel: Phase transformations and mechanical properties, Materials and Design, 56 (**2014**), 258–263, doi:10.1016/j.matdes.2013.11.022

[4] S. Anttila, P. Karjalainen, S. Lantto, Mechanical properties of ferritic stainless steel welds in using type 409 and 430 filler metals, Welding in the World, 57 (**2013**), 335–347, doi:10.1007/s40194-013-0033-7

[5] C. C. Silva, J. P. Fariasa, H. C. Miranda, R. F. Guimarãesa, J. W. A. Menezesb, M. A. M. Neto, Microstructural characterization of the HAZ in AISI 444 ferritic stainless steel welds, Materials Characterization, 59 (**2008**) 5, 528–533, doi:10.1016/j.matchar.2007.03.011

[6] A. K. Lisiecka, A. Lisiecki, Laser welding of the new grade of advanced high-strength steel Domex 960, Mater. Tehnol., 51 (**2017**) 2, 199–204, doi:10.17222/mit.2015.158

[7] K. M. Hong, Y. C. Shin, Prospects of laser welding technology in the automotive industry: A review, Journal of Materials Processing Technology, 245 (**2017**), 46–69, doi:10.1016/j.jmatprotec.2017.02.008

[8] M. P. Prabakaran, G. R. Kannan, Optimization of laser welding process parameters in dissimilar joint of stainless steel AISI316/AISI1018 low carbon steel to attain the maximum level of mechanical properties through PWHT, Optics and Laser Technology, 112 (**2019**) 15, 314–322, doi:10.1016/j.optlastec.2018.11.035

[9] S. Chatterjee, S. S. Mahapatra, V. Bharadwaj, B. N. Upadhyay, K. S. Bindra, J. Thomas, Parametric appraisal of mechanical and metallurgical behavior of butt welded joints using pulsed Nd:YAG laser on thin sheets of AISI 316, Optics and Laser Technology, 117 (**2019**), 186–199, doi:10.1016/j.optlastec.2019.04.004

[10] L. Cao, Y. Yang, P. Jiang, Q. Zhou, G. Mi, Z. Gao, Y. Rong, C. Wang, Optimization of processing parameters of AISI 316L laser welding influenced by external magnetic field combining RBFNN and GA, Results in Physics, 7 (**2017**), 1329–1338, doi:10.1016/j.rinp.2017.03.029

[11] M. Ragavendran, N. Chandrasekhar, R. Ravikumar, R. Saxena, M. Vasudevan, A. K. Bhaduri, Optimization of hybrid laser–TIG welding of 316LN steel using response surface methodology (RSM), Optics and Lasers in Engineering, 94 (**2017**), 27–36, doi:10.1016/j.optlaseng.2017.02.015

[12] P. Jiang, C. Wang, Q. Zhou, X. Shao, L. Shu, X. Li, Optimization of laser welding process parameters of stainless steel 316L using FEM, Kriging and NSGA-II, Advances in Engineering Software, 99 (**2016**), 147–160, doi:10.1016/j.advengsoft.2016.06.006

[13] A. Torabi, F. Kolahan, Optimizing pulsed Nd:YAG laser beam welding process parameters to attain maximum ultimate tensile strength for thin AISI316L sheet using response surface methodology and simulated annealing algorithm, Optics & Laser Technology, 103 (**2018**), 300–310, doi:10.1016/j.optlastec.2017.12.042

[14] K. Y. Benyounis, A. G. Olabi, M. S. J. Hashmi, Effect of laser welding parameters on the heat input and weld-bead profile, Journal of

Materials Processing and Technology, 164–165 (**2006**) 15, 978–985, doi:10.1016/j.jmatprotec.2005.02.060

[15] H. Vahiddastjerdi, A. Rezaeian, M. R. Toroghinejad, G. Dinib, E. Ghassemali, Optimizing pulsed Nd: YAG laser welding of high-Mn TWIP steel using response surface methodology technique, Optics & Laser Technology, 120 (**2019**) 105721, doi:10.1016/j.optlastec.2019.105721

[16] A. G. Olabi, F. O. Alsinani, A. A. Alabdulkarim, A. Ruggiero, L. Tricarico, K. Y. Benyounis, Optimizing the CO2 laser welding process for dissimilar materials, Optics and Lasers in Engineering, 51 (**2013**) 7, 832–839, doi:10.1016/j.optlaseng.2013.01.024

[17] N. Kumar, M. Mukherjee, A. Bandyopadhyay, Comparative study of pulsed Nd:YAG laser welding of AISI304 and AISI 316 stainless steels, Optics & Laser Technology, 88 (**2017**), 24–39, doi:10.1016/j.optlastec.2016.08.018

[18] M. R. Pakmanesh, M. Shamanian, Optimization of pulsed laser welding process parameters in order to attain minimum underfill and undercut defects in thin 316L stainless steel foils, Optics & Laser Technology, 99 (**2018**), 30–38, doi:10.1016/j.optlastec.2017.09.047

[19] A. A. Narayanan, R. S. Sudheesh, Optimization of tribological properties of an epoxy hybrid polymer composite reinforced with ZrB_2 and PTFE particles using response surface methodology for high-temperature tribological applications, Mater. Tehnol., 55 (**2021**) 6, 799–807, doi:10.17222/mit.2021.239

[20] M. T. Mao, H. J. Guo, F. Wang, X. L. Sun, Effect of Cooling Rate on the Solidification Microstructure and Characteristics of Primary Carbides in H13 Steel, ISIJ International, 59 (**2019**) 5, 848–857, doi:10.2355/isijinternational.ISIJINT-2018-524

[21] P. V. S. Lakshminarayana, J. P. Gautam, P. Mastanaiah, G. M. Reddy, K. B. S. Rao, Influence of beam power and traverse speed in fibre laser welding of dual phase steel (590) on depth of weld zone penetration, microstructure and hardness, Materials Today: Proceedings, 5 (**2018**) 9, 17132–17138, doi:10.1016/j.matpr.2018.04.121